Well integrity for CO_2 injection from ships: Simulation of the effect of flow and material parameters on thermal stresses

Peder Aursand[a], Morten Hammer[a], Alexandre Lavrov[b], Halvor Lund[a,*], Svend Tollak Munkejord[a], Malin Torsæter[b]

[a]*SINTEF Energy Research, P.O. Box 4761 Sluppen, NO-7465 Trondheim, Norway*
[b]*SINTEF Petroleum Research, P.O. Box 4763 Sluppen, NO-7465 Trondheim, Norway*

Abstract

Ships have been shown to be the most cost-effective way to transport CO_2 from many sources in the Nordic region to offshore storage sites. Injection from ships introduces new challenges for the integrity of CO_2 injection wells. The low temperature and the intermittency of CO_2 injected from ships give rise to large temperature variations in the well. Such variations may lead to thermal stresses that exceed the limits of the well construction method and materials.

In this paper we present a coupled flow and heat conduction model for CO_2 wells. The model is used to conduct a parameter study and determine the parameters' effect on the temperature variations in the well during injection from ships. The parameters varied are injection rate, injection time, injection temperature and time between injections. The resulting temperature variations are used as input for a 2D thermoelastic finite-element model in ABAQUS to determine the thermal stresses. Our results show that the amplitude of temperature variations downhole is mainly increased by longer pauses between injections, and by lower injection temperature. In the worst-case scenario considered in this paper, the thermal stresses may be large enough to induce debonding at the casing–cement interface.

Keywords: CO_2 injection wells, two-phase flow, well integrity, heat conduction, thermal cycling, thermal stresses

1. Introduction

CO_2 Capture and Storage (CCS) will require large storage volumes for CO_2. Both onshore and offshore storage options are considered in Europe. Storage in saline aquifers beneath the North Sea is considered an attractive option, due to large available storage volumes and public resistance against onshore storage. For example, the Utsira formation alone has an estimated storage capacity of 40 Gt (Lindeberg *et al.*, 2009).

The Norwegian Government aims to realize full-scale CCS demonstration in Norway by 2020, and a pre-feasibility study was concluded in May 2015 (Norwegian Ministry of Petroleum and Energy, 2015). An outcome of this study was the selection of three candidates for onshore capture located in near proximity to the sea in the south-east part of Norway. This includes a Waste-to-Energy plant in Oslo (Klemetsrud), a cement factory in Brevik (Norcem) and an ammonia plant in Porsgrunn (Yara). The current approximate annual emissions from these locations, and thus the potential for capture is 400 kt for Klemetsrud, 800 kt for Norcem and 600 kt for Yara. Another conclusion from this pre-feasibility study is that ship transport will be the most cost-effective.

---

[*]Corresponding author.
Email addresses: `peder.aursand@gmail.com` (Peder Aursand), `morten.hammer@sintef.no` (Morten Hammer), `alexandre.lavrov@sintef.no` (Alexandre Lavrov), `halvor.lund@sintef.no` (Halvor Lund), `svend.t.munkejord@sintef.no` (Svend Tollak Munkejord), `malin.torsater@sintef.no` (Malin Torsæter)

Following the pre-feasibility study, a feasibility study was launched early in 2016 (Norwegian Ministry of Petroleum and Energy, 2016). The feasibility study includes assessment of three possible storage sites on the Norwegian Continental Shelf (Utsira, Smeaheia and Heimdal).

Ships represent a flexible transport solution for transporting CO_2 from many sources to an offshore storage site. Kjärstad et al. (2015) found that for most sources in the Nordic region, ship transport was cheaper than pipelines. Ships are especially useful for small sources that are located far away from the storage site (Vermeulen, 2011). CO_2 ships may be unloaded either on a common onshore hub, as suggested by e.g. Mazzetti et al. (2015), or directly to an offshore unloading platform (Aspelund et al., 2006). The advantages of an onshore hub include less weather dependent unloading and less equipment on each ship, which reduces the ship cost. It does, however, require a long pipeline to be built from the hub to the storage site.

CO_2 transport by ship introduces some challenges compared to pipelines. One important aspect is the CO_2 liquefaction process (Brownsort, 2015), which should be integrated with the CO_2 capture and conditioning processes. If CO_2 is injected from a ship at an offshore unloading point without buffer capacity, the injection will be intermittent, since injection stops when the ship is finished unloading. Such intermittent injection can have a number of detrimental effects on the well and the reservoir. First, research indicates that low injection rates, such as those occurring during intermittent CO_2 injection, can be detrimental to CO_2 injectivity into saline aquifers (Kim et al., 2012; Giorgis et al., 2007). Second, CO_2 injected from a ship will typically have a much lower temperature than the reservoir into which it is injected. Intermittent injection will then lead to large temperature fluctuations, which in turn induces thermal stresses in the well and reservoir (De Andrade et al., 2014; Lund et al., 2016).

Thermal stresses can affect the sealing ability of well barriers – steel casing, cement and rock formation. These barriers can fail individually (e.g. by cracking of cement), or the bond between them can fail. The latter has been demonstrated to be a real problem in both laboratory and field studies (Carey et al., 2007; Crow et al., 2010; Kjøller et al., 2016), and is a major concern when it comes to CO_2 well integrity. The integrity of the interfaces between cement–casing and cement–rock is most severely threatened in situations where the well is exposed to strong temperature variations (Manceau et al., 2015; Nygaard et al., 2014; Bois et al., 2010). In this paper we seek to uncover when such critical situations can occur during CO_2 injection.

In addition to affecting the cement interfaces, cooling-induced thermal stresses in the casing string may inadvertently affect the casing itself. In particular, tensile axial stress in the casing caused by cooling-induced contraction may affect the integrity of the couplings (Maharaj, 1996). These effects, however important they may be, were not considered in this study.

Another cooling-related issue in CO_2 storage resevoirs are thermal stresses in the rock itself (Søreide et al., 2014; Holt et al., 2016). Cooling reduces the compressive in-situ stresses in the reservoir, which may reduce the fracture gradient during drilling, facilitate fracturing during CO_2 injection, and possibly promote subsidence. Whether these effects are local (near-well) or reservoir-wide is still an open question and needs dedicated studies, both theoretical and experimental.

In order to ensure efficient and safe design and operation of offshore CO_2 injection systems, transient flow models constitute an important tool. Such models need to take into account single- and multiphase flow of CO_2 and CO_2-rich mixtures in horizontal and vertical configurations, including such effects as friction and heat transfer. Data and models for thermophysical properties and flow of CO_2 and CO_2-rich mixtures were reviewed by Munkejord et al. (2016).

Cronshaw and Bolling (1982) developed a finite-difference model for single- or two-phase flow of CO_2 in wellbores. A semi-implicit time-integration procedure was employed. Heat conduction to the surroundings was accounted for, and the thermophysical properties were taken from look-up tables. The flow transients were assumed to be slow enough that kinetic-energy changes across control volumes could be neglected.

Pan et al. (2009) considered a transient drift-flux model (DFM) for two-phase CO_2-brine mixtures to quantify potential leakages up wells. A DFM was also studied by Lu and Connell (2014b,a). The Peng and Robinson (1976) equation of state (EOS) was used, assuming full thermodynamic equilibrium. The effect of transient boundary conditions at the well inlet was included.

Ruan et al. (2013) studied the effect of water convection in the annulus surrounding the well assuming 2D axisymmetry. Musivand Arzanfudi and Al-Khoury (2015) modelled the leakage of CO_2 through an air-filled

abandoned wellbore using a mixed finite-element discretization scheme. The main aim was to achieve a high numerical efficiency.

de Koeijer *et al.* (2014) pointed out that there is a need for experiments on shut-ins and depressurization in CO_2 injection wells. A main point of interest was stated to be the interaction between CO_2 and brine in the reservoir. It was suggested to construct a new infrastructure, drilling a 200–250 m deep well.

We have developed a 1D multiphase transient flow model for CO_2 and CO_2-rich mixtures, using drift-flux and two-fluid flow-model formulations (Munkejord *et al.*, 2010; Munkejord and Hammer, 2015). The main application has been fast transients in pipelines, but the model has also been employed to describe somewhat longer-duration transients (Aursand *et al.*, 2016) and flow in wells (Linga and Lund, 2016).

Linga and Lund (2016) considered blow-out and shut-in scenarios. In the present paper, we aim to investigate how different CO_2 injection cycles affect the temperature in an injection well, and how this affects the sealing ability of well barrier materials. This may be a function of a number of parameters, such as the thermal properties of the well materials, the temperature and pressure as well as thermophysical properties of the injected CO_2, the injection rate and whether the injection is intermittent or not. The heat transfer to the surroundings is calculated using the multilayer conduction model discussed by Lund *et al.* (2016). The resulting well-casing temperature is then imposed as a boundary condition in a separate finite-element calculation, enabling us to estimate the stresses at the material interfaces in the well. For well integrity to be maintained, it is important that the stresses do not exceed the limits set by the construction method and materials.

The rest of this paper is organized as follows. In Section 2, the homogeneous equilibrium model with heat conduction to the surroundings is briefly described. Section 3 summarizes the employed numerical methods. In Section 4, the flow model is validated against CO_2 well-flow data from Cronshaw and Bolling (1982). Section 5 discusses the most relevant parameters for the present CO_2 injection case study. In Section 6, we present simulation results from the flow model, which are then fed into a finite-element simulator to estimate the temperature-induced stresses at the material interfaces in the well. Conclusions are drawn in Section 7.

2. Fluid flow model

CO_2 flow in the injection well is modelled using a two-phase homogeneous equilibrium model with friction and radial heat transfer. The reference equation of state for CO_2 from Span and Wagner (1996) is applied within the model.

2.1. Homogeneous equilibrium model

We consider a fluid composed by two phases $k \in \{g, \ell\}$ (gas and liquid), such that the volume fractions $\alpha_k \in [0, 1]$ satisfy

$$\sum_k \alpha_k = 1. \tag{1}$$

The flow is one dimensional in a vertically oriented pipe (the tubing), where we take the x-axis to be oriented downwards. The governing equations, found through averaging methods (Drew and Passman, 1999) and by assuming instantaneous equilibrium in pressure, temperature, chemical potential and velocity, are then given by

$$\frac{\partial}{\partial t}\rho + \frac{\partial}{\partial x}\rho v = 0, \tag{2a}$$

$$\frac{\partial}{\partial t}\rho v + \frac{\partial}{\partial x}(\rho v^2 + p) = \rho g - f_{\text{wall}}, \tag{2b}$$

$$\frac{\partial}{\partial t}E + \frac{\partial}{\partial x}v(E + p) = \rho v g + Q, \tag{2c}$$

3

representing mass conservation and momentum and total-energy balance. Herein, v is the velocity, p is the pressure, and we have introduced the mixture density

$$\rho = \sum_k \alpha_k \rho_k, \tag{3}$$

and the mixture total energy

$$E = \rho v^2 / 2 + \sum_k \alpha_k \rho_k e_k. \tag{4}$$

The gravitational acceleration in the direction of the pipe is g. The term f_{wall} accounts for the friction between the fluid and the wall. Herein, we employ the Friedel (1979) friction model .

2.2. Heat conduction model

The heat flux per fluid volume, Q, is introduced to account for the radial heat conduction into the tubing. Q is time-dependent, and given by

$$Q = \frac{2}{r_i} h_i (T_w - T) \tag{5}$$

where r_i is the tubing inner radius, h_i is the fluid–wall heat transfer coefficient and T_w is the temperature of the tubing inner wall. T_w is calculated by coupling the flow model to the radial heat equation (Cannon, 1984),

$$\rho(r) c_p(r) \partial_t T(r, t) = \frac{1}{r} \partial_r (r \kappa(r) \partial_r T(r, t)) . \tag{6}$$

The equation (6) is solved for n concentric thermal layers consisting of the tubing and the different materials encasing it. Here, $\kappa(r)$, $\rho(r)$ and $c_p(r)$ are the thermal conductivity, density and heat capacity, respectively, at radius r. For instance, $\kappa(r)$ takes the form

$$\kappa(r) = \begin{cases} \kappa_1, & \text{if } r_0 \leq r < r_1, \\ \quad \vdots \\ \kappa_n, & \text{if } r_{n-1} \leq r \leq r_n, \end{cases} \tag{7}$$

where r_i is the outer radius of layer i.

2.3. Thermophysical properties

We assume locally full thermodynamic equilibrium. The Span–Wagner equation of state is used to solve the energy–density flash problem for the mixture density and specific internal energy,

$$e = \frac{1}{\rho} \sum_k \alpha_k \rho_k e_k. \tag{8}$$

Pressure, temperature and phase distribution is solved by choosing the phase composition—single-phase gas, single-phase liquid, or two-phase mixture—which maximizes the mixture entropy

$$S = \sum_k \alpha_k \rho_k s_k. \tag{9}$$

The numerical approach is described in detail by Giljarhus *et al.* (2012) and Hammer *et al.* (2013).

In this work, the CO_2 viscosity is calculated using the correlation of Fenghour *et al.* (1998), and the thermal conductivity is calculated by the correlation of Vesovic *et al.* (1990).

3. Numerical method

In this section we briefly describe the numerical methods used for solving the model presented in the previous section.

3.1. Finite-volume method

The heat conduction equation (6) is solved using a finite-volume scheme as described by Lund *et al.* (2016). The flow equations (2) are also discretized spatially using a finite-volume scheme. We employ a second-order MUSCL (Monotonic Upstream-Centered Scheme for Conservation Laws) reconstruction with a minmod limiter (see e.g. LeVeque (2002)) in each finite volume, where we reconstruct ρ, E and v linearly. For the numerical flux between cells, we use the centred FORCE (first-order centered) flux (Toro and Billett, 2000). For time integration, we use the strong-stability preserving two-stage second-order Runge–Kutta method (Gottlieb *et al.*, 2001). The employed computational fluid dynamics method has been developed and validated in a series of papers (see Munkejord *et al.*, 2010; Hammer *et al.*, 2013; Hammer and Morin, 2014; Munkejord and Hammer, 2015; Munkejord *et al.*, 2016).

3.2. Boundary conditions

In this work, three kinds of boundary conditions are applied to the fluid flow model (2): stationary wall, specified mass flow rate, and reservoir injection. Boundary conditions are applied in one of two ways. The first is to impose a numerical flux at the edge of the domain. The second is to set the solution value in a ghost cell – an extra cell outside the physical domain – which is used when calculating the numerical FORCE flux on the edge of the domain.

3.2.1. Stationary wall

The stationary wall boundary condition is imposed by extrapolating all quantities except velocity from the inner domain to the ghost cell. The velocity is inverted, which ensures no mass flux through the wall.

3.2.2. Mass flow rate

The mass flow rate boundary condition is applied by setting the numerical flux at the edge of the domain. The numerical flux is given by eq. (2) as

$$F = \begin{pmatrix} \rho v \\ \rho v^2 + p \\ v(E + p) \end{pmatrix}. \tag{10}$$

In our boundary condition, the mass flux ρv and the temperature are prescribed, whereas the pressure is extrapolated from the inner domain. A pressure–temperature flash is then used to calculate density and energy used in the numerical flux.

3.2.3. Reservoir injection

The reservoir is characterized by an injectivity I, which determines the bottomhole pressure as a function of injection rate. This can be formulated as

$$p_{\text{bottomhole}} = \frac{\rho v A}{I} + p_{\text{reservoir}}, \tag{11}$$

where A is the flow area, and $p_{\text{reservoir}}$ is the reservoir pressure. In our numerical scheme, we apply the reservoir boundary condition by setting $p_{\text{bottomhole}}$ in the ghost cell according to eq. (11). The entropy and the velocity of the flow are extrapolated from the inner domain. A pressure–entropy flash is then used to calculate density and energy used in the ghost cell.

Table 1: Parameters for model validation

Quantity	Value
Well length	914.4 m
Deviation angle	26.5 degrees
Gravity along well axis	8.78 m/s^2
Tubing inner diameter	8.83 cm
Tubing roughness	4.572×10^{-6} m
Relative roughness	5.2×10^{-5}

(a)

(b)
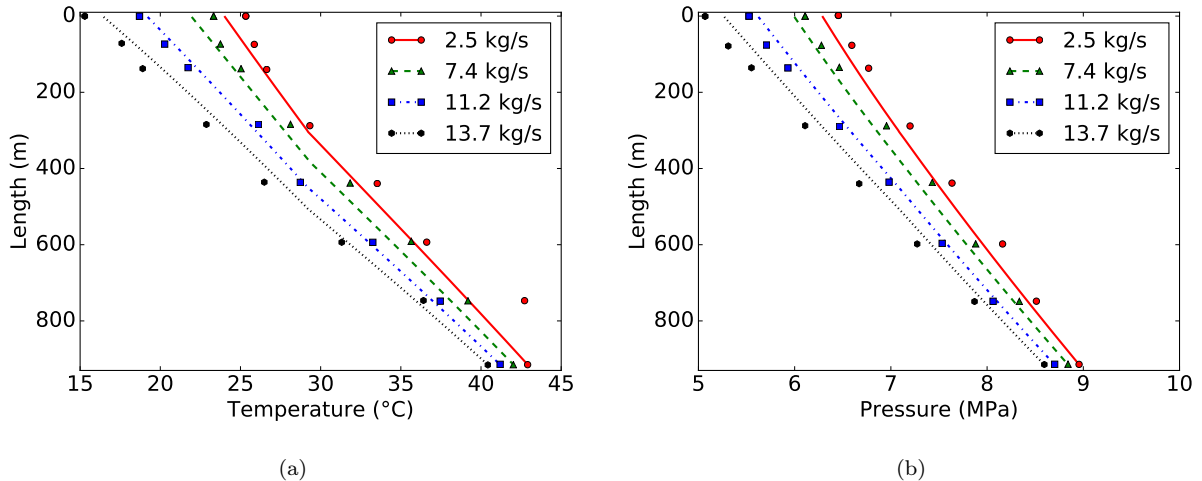
Figure 1: Our simulation results (lines) and measurements from Cronshaw and Bolling (1982) (markers) for a CO_2 production well

4. Validation of the flow model

Cronshaw and Bolling (1982) presented experimental data for temperature and pressure in a CO_2 production well for various flow rates. The well produces 97% CO_2, the remaining 3% are unspecified. We nevertheless attempt to apply our model for pure CO_2 to this well, as a means of validating our model. Cronshaw and Bolling (1982) stated that after half a day of production (and maybe even earlier), the well-head conditions no longer vary. This is because heat transfer to the surroundings is much smaller than the (forced) heat convection in the fluid at this point. We therefore apply our model without any heat transfer to the surroundings.

Table 1 shows relevant parameters for the production well. The measured bottomhole pressure and temperature are used as inlet boundary conditions for the model, whereas the massflow is used as an outlet condition. The model is time-stepped until steady state is reached.

Figure 1 shows the temperature and pressure in the well for the four different flow rates presented by Cronshaw and Bolling (1982). Our simulation results (lines) match reasonably well with the measurements (markers), especially when one considers that we do not know the exact fluid composition. The maximum absolute error in temperature is 3.5 °C and 0.23 MPa in pressure. For the flowrate 2.5 kg/s, there seems to be a temperature outlier at 800 m. If this outlier is removed, the maximum error in temperature is reduced to 1.4 °C. For comparison, the model of Cronshaw and Bolling (1982) had errors of 1.7 °C in temperature and 0.21 MPa in pressure. This also seems to be without the temperature outlier. Lu and Connell (2008) also used these measurements to validate their model (employing the Peng–Robinson EOS), and obtained errors of 4.2 °C and 0.4 MPa.

5. Parameters for the case study

In this section, we review the valid ranges for injection parameters relevant for a ship-based CO_2 injection scenario in the North Sea. As this study focuses on the thermal stresses induced by periodic injection of liquid CO_2 in an injection well, certain simplifying assumptions are made which are not expected to significantly affect the large-time-scale heat transport.

5.1. Injection rate

Practical CO_2 well injection rates will vary greatly depending on the source, the delivery system (ship or pipeline) as well as the injectivity and capacity of the target reservoir. The CO_2 injection well at Sleipner in the North Sea uses a pipeline delivery system and has a reported injection rate of 28.7 kg/s (Thu, 2013). Kjärstad *et al.* (2015) used injection rates of up to 4 Mtpa (126 kg/s) per well in their examples, but it is not clear if such a high rate is possible in practice. Vermeulen (2011) suggested 450 kg/s divided on three wells for injection from ships. Mazzetti *et al.* (2015) argued for an injection rate of 3 Mtpa (95 kg/s) for the Utsira formation.

For pipeline-based injection scenarios, injection rates are commonly quoted in Mtpa, assuming a near-steady injection. It is important to note that, depending on the docking cycle, ship based injection with a comparable net annual injection may imply significantly higher injection flow rates. In particular, weather and ocean conditions can prevent long-term continuous docking at the injection site, which means that large flow rates will be required in order to inject significant volumes of CO_2.

There might be limitations to the injection rates allowing for a sustainable operation of an injection well. Luo and Bryant (2013) discussed the limits on injection rates due to possible fracturing due to thermo-elastic stresses. The report by Whiriskey (2014) concluded that the Sleipner CO_2 well is in the upper injectivity range, and suggests using an injectivity of 0.6 Mtpa (19 kg/s).

Based on the limited available data for ship-based CO_2 injection and the practical consideration above, we will in this work perform numerical experiments with injection rates in the range 25–100 kg/s.

5.2. Injection time

The injection time during ship-borne CO_2 injection is influenced by the ship's capacity, its maximum flow rate, injectivity constraints of the well, as well as operational concerns such a weather and sea conditions. Vermeulen (2011) suggested 24 h unloading for a 30,000 m^3 ship. Depending on buoy solution and local weather and sea conditions, ships may not be able to consistently dock for longer periods of time than this. In their report, Kjärstad *et al.* (2015) used 54 hours for offloading (including connections to offloading buoy) from a ship of 40,000 m^3. Both these reports suggested transporting CO_2 at 7 bar and −50 °C, which maximizes the density of the CO_2.

Based on the information available, we will carry out numerical experiments with injection times of 24–48 h. With injection rates in the range 25–100 kg/s, this corresponds to a total ship CO_2 volume per cycle of 1870–14,961 m^3 (assuming transport conditions of −50 °C and 8 bar, giving a liquid density of 1155 kg/m^3).

For the down-time between injections, the report by Kjärstad *et al.* (2015) indicated that the time needed to connect and disconnect from an offloading buoy should be less than 10 h for a ship of 40,000 m^3. In our case study we use injection pause times of 8–24 h. Here, the lower end corresponds to a relatively continuous stream of transport ships where the only down-time is for switching connections.

5.3. Injection composition

While the CO_2 stream used for injection at Snøhvit is near pure (> 99%) (Moumets *et al.*, 2015), this may not always be the case in practical injection scenarios. Depending on the source, CO_2 for injection can contain significant amounts of impurities. The presence of even small quantities of impurities in a CO_2 stream can affect its thermodynamic properties. In particular, as discussed e.g. by Paterson *et al.* (2008), if the presence of impurities shifts the critical point of the mixture, two-phase conditions are more likely to be encountered.

However, it is unlikely that impurities will effect the transport of heat during what is mostly a single-phase injection. In addition, CO_2 transported by ships is likely to be very pure, since this is required

Table 2: Solubility of some volatile impurities in liquid CO_2 at $-47\,°C$ and $8\,bar$.

Impurity	Solubility (ppm)
N_2	408.8
Ar	621.7
O_2	580.1
CO	646.6
H_2	91.25
CH_4	1281

for condensing CO_2 to low temperatures. Impurities more volatile than CO_2 will have low solubility at low temperatures, and water must be removed to avoid hydrate and ice formation. The solubility of some volatile impurities possibly found in CO_2 at $8\,bar$ and $-47\,°C$ are listed in Table 2. The condition is selected as a slightly sub-cooled state of pure CO_2 at $8\,bar$, having a saturation temperature of $\approx -46\,°C$.

In light of these considerations, we will in this case study consider pure CO_2 in order to simplify the fluid calculations involved.

5.4. Injection temperature

It is highly likely that CO_2 transported by ships must be heated before being pumped into the well. Injection at temperatures close to or below freezing introduce higher risk of thermal stress in the tubing and casing. As discussed by Aspelund *et al.* (2006), heating CO_2 by using sea water directly might not be feasible in a North Sea injection scenario, since the heat exchangers would freeze due to the low sea water temperature. In the current case study we will consider injection temperatures in the range from $4.85\,°C$ (approximate sea temperature) to $19.85\,°C$ (CO_2 heated somewhat above sea temperature). It should be noted that heating CO_2 to $19.85\,°C$ after low temperature ship transport might be unrealistic since it would require significant heating power. For reference, the wellhead temperature at Snøhvit is about $4\,°C$ (Moumets *et al.*, 2015), and at Sleipner around $25\,°C$.

5.5. Injection well and reservoir

The Snøhvit reservoirs used for CO_2 injection, Tubåen and Stø, are $2600\,m$ and $2450\,m$ deep, respectively (Moumets *et al.*, 2015). The Sleipner CO_2 well is around $1000\,m$ deep (Krogh *et al.*, 2012; Lindeberg, 2011; Thu, 2013), but is strongly deviating and extends horizontally, the tubing itself being around $3000\,m$ long. While the slope and horizontal extent of the injection well can have important implications for flow assurance, it is not expected to have significant impact on the fluid-to-pipe heat transport during steady-state conditions. For simplicity we will therefore assume a perfectly vertical injection well with a depth of $1500\,m$.

An injection well is made up of a number of concentric layers of different materials, each with different thermal properties. In practice, the layers may not be perfectly concentric, but in this work we assume so. We assume a geometry illustrated in Figure 2 with physical and thermal properties given in Table 3. In particular, we assume that the casing is surrounded by drilling mud for the top $1400\,m$, while cement is used in the bottom $100\,m$.

The vertical thermal gradients in the rock and soil can be quite large in the North Sea, and they have been quoted to be $41\,°C/km$ (Lindeberg, 2011). In the present case study we assume a linearly increasing formation temperature from $4\,°C$ at the surface to $65\,°C$ at a depth of $1500\,m$. It should be noted that this thermal gradient is among the highest reported in the North Sea, but this can be considered a worst case for temperature variations in the well.

For the reservoir injectivity we use a constant value of $8.7 \times 10^{-5}\,kg/(s\,Pa)$, which is the estimated value for the Sleipner well (Thu, 2013). The overall injection well and reservoir parameters are summarized in Table 4.

Table 3: Material properties and dimensions for the layers surrounding the fluid flow.

| Item	Radial segment [cm]	Axial segment [km]	Density [kg/m³]	Thermal conductivity [W/(m K)]	Specific heat capacity [J/(kg K)]
Tubing (ST 52-3) (Albawi, 2013)	8.5–9.0	0–1.5	7850	40	500
Packer fluid (Halliburton, 2012)	9.0–11.1	0–1.5	1400	0.26	4000
Casing (ST 52-3) (Albawi, 2013)	11.1–12.2	0–1.5	7850	40	500
Drilling mud (Bjørkevoll, 2014)	12.2–15.5	0–1.4	1500	0.8	2500
Cement (Portland Class G) (Albawi, 2013)	12.2–15.5	1.4–1.5	1917	0.72	780
Caprock/shale (Eppelbaum *et al.*, 2014; Gilliam and Morgan, 1987)	15.5–500	1.4–1.5	2057	1.0	1000
Sandstone (Castlegate) (Albawi, 2013)	15.5–500	0–1.5	2600	2.0	1000
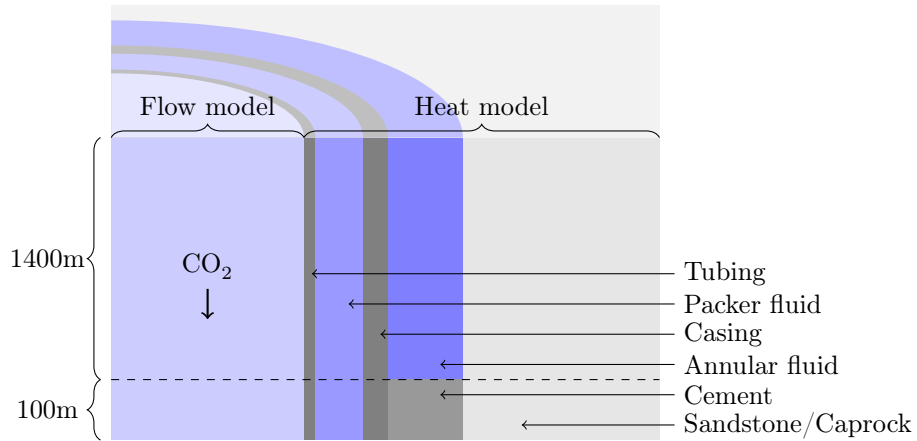
Figure 2: A simplified illustration of the bottom of the well showing the radial layers. The radial segments are to scale, but the axial segments are not. The blue layers are fluid, while the grey ones are solid. In the bottom $100\,\mathrm{m}$ of the well, the annular fluid is replaced with cement. Also, in one simulation, caprock is used as the outer radial segment for the bottom $100\,\mathrm{m}$.

Table 4: Injection well and reservoir parameters used for case study.

Quantity	Value
Well depth	$1500\,\mathrm{m}$
Formation temperature	$65\,°\mathrm{C}$
Thermal gradient	$41\,°\mathrm{C/km}$
Injectivity	$8.7 \times 10^{-5}\,\mathrm{kg/(s\,Pa)}$
Gravity	$9.81\,\mathrm{m/s^2}$
Relative pipe roughness	5×10^{-5}

9

6. Results

This section presents results from our coupled fluid-dynamics and thermal simulations, as well as a study employing the simulated temperatures as a boundary condition in finite-element simulations in order to evaluate the stresses at the material interfaces in the well.

6.1. The effect of injection parameters on casing temperature

Simulations were performed to investigate the effect of the following parameters on the temperature evolution in the well materials:

- **Flow rate**: The injection flow rate.

- **Temperature**: The temperature of the CO_2 at the wellhead.

- **Injection cycle**: The duration of the injection and down-time.

- **Effect of caprock**: The influence of a caprock layer on the bottomhole temperatures.

The study is performed using constant well parameters, given in Table 4. For the numerical solution, we use 100 computational cells in the axial direction (flow model) and 100 computational cells to resolve the radial heat transfer. A Courant number of 0.3 was used in all fluid computations. The thermal properties of the concentric layers making up the well are given in Table 3. Due to the casing's potential vulnerability to thermal stress, the casing temperature (and its time evolution) is used as the main target variable in this parameter study.

Figure 3 shows the temperature evolution in the casing at a point near the bottom of the well (1450 m) for different injection parameters. As expected, the temperature variations are greatest for high flow rates combined with low injection temperatures. One can also observe that longer down-time between injections will significantly affect the magnitude of the temperature recovery in the casing. The highest fluctuation in casing temperature between cycles can be seen for 48 h injection and 24 h down-time (Figure 3d). Herein, the fluctuation varies from about 5 °C when injecting 19.85 °C CO_2 at 25 kg/s to about 15 °C when injecting 4.85 °C CO_2 at 100 kg/s.

Figure 4 shows the fluid temperature and pressure profiles as a function of well depth at the initial time, after a 48 h injection, and after a subsequent 24 h pause. A comparison is made between injection at 4.85 °C and 19.85 °C. The vertical temperature gradient is clearly higher in the two-phase region closest to the well head compared to the single-phase conditions prevalent in the deeper parts of the injection well. The results clearly indicate that over an injection cycle the largest absolute temperature fluctuations can be found near the bottom of the well, making this the well segment most susceptible to thermal stress. During injection, the bottomhole pressure is about 160 bar for the highest injection rate (100 kg/s), which is around 10 bar higher than the reservoir pressure. Reducing the injection rate to 25 kg/s, gives a 7 bar lower bottomhole pressure. The wellhead pressure lies in the range 40–60 bar, which is slightly lower than the wellhead pressure at Sleipner (Thu, 2013).

In order to study the effect of the caprock layer on the temperature cycle, simulations were carried out using 48 h injection of 4.85 °C CO_2 injected at a rate of 100 kg/s followed by a 24 h pause. A layer of caprock with thermal properties given in Table 3 is introduced replacing the sandstone in the bottom 100 m of the injection well. The temperature evolution in the casing at 1450 m, shown in Figure 5, demonstrates a significant decrease for caprock compared to sandstone. However, the potentially harmful temperature variation remains almost identical.

The casing temperature is particularly sensitive to the interval lengths of the injection cycle, as shown in Figure 6. Here, different injection cycles were simulated using 4.85 °C CO_2 injected at a rate of 100 kg/s, corresponding to the *worst case* injection parameters inferred from Figure 3. By worst case we mean the case with the largest amplitude of downhole temperature variations. Within the parameter space studied here, the injection time does not significantly influence the minimum casing temperature. A 24 h injection lasts sufficiently long to cool the fluid, tubing and casing to what seems to be a quasi-steady state. However, since the heating process, which occurs when injection is stopped, is slower than the cooling when injecting,
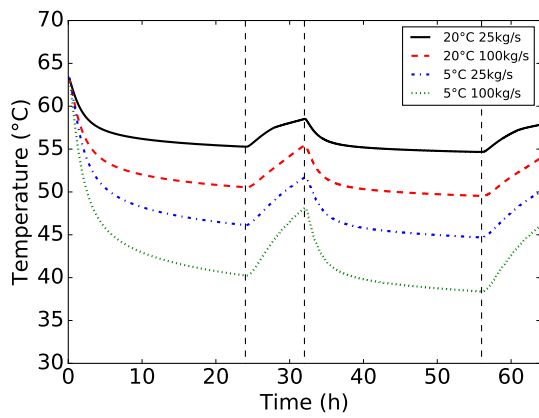
(a) 24 h injection, 8 h pause
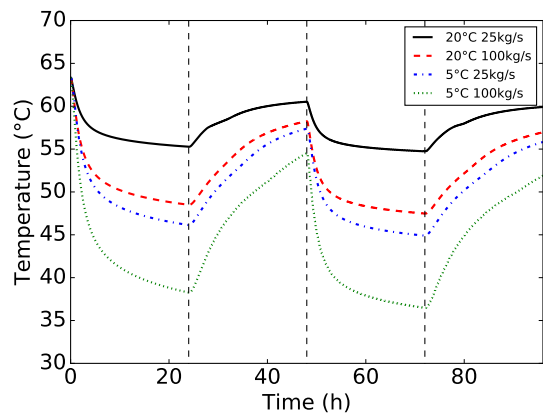
(b) 24 h injection, 24 h pause
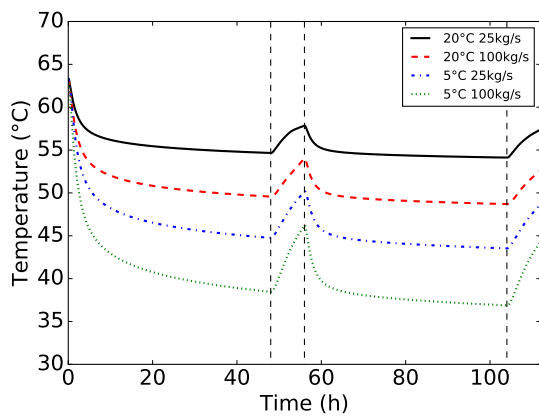
(c) 48 h injection, 8 h pause
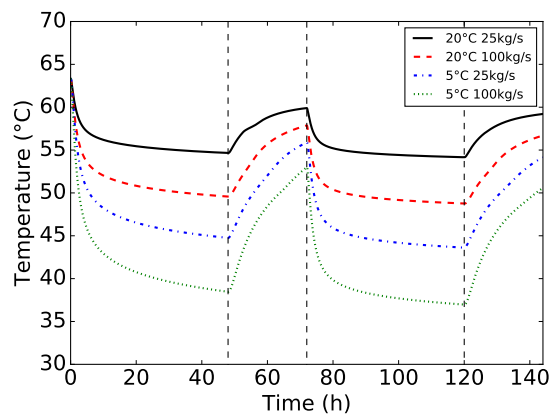
(d) 48 h injection, 24 h pause

Figure 3: The casing temperature at 1450 m as a function of time for different injection cycles, injection temperatures, and injection flow rates.
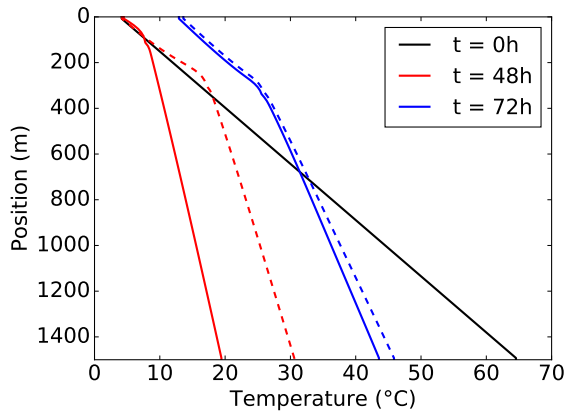
(a) Temperature, injection at $4.85\,^{\circ}\mathrm{C}$
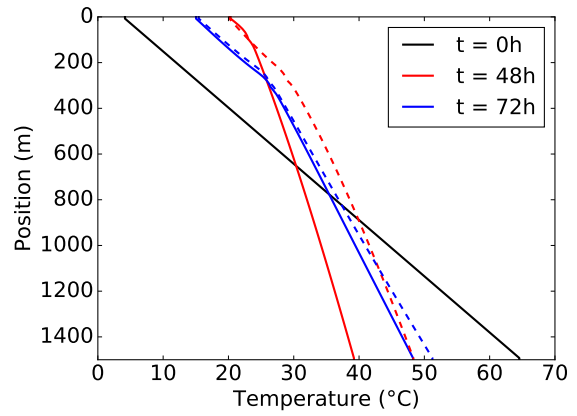
(b) Temperature, injection at $19.85\,^{\circ}\mathrm{C}$
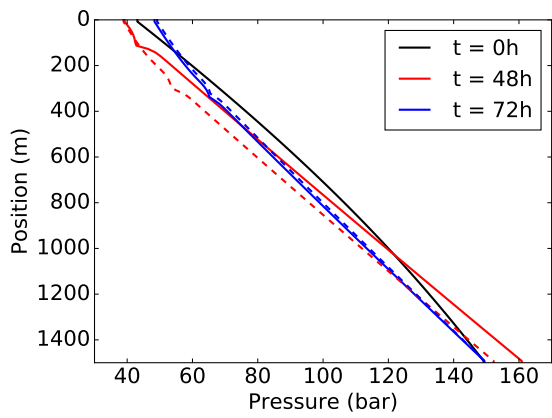
(c) Pressure, injection at $4.85\,^{\circ}\mathrm{C}$
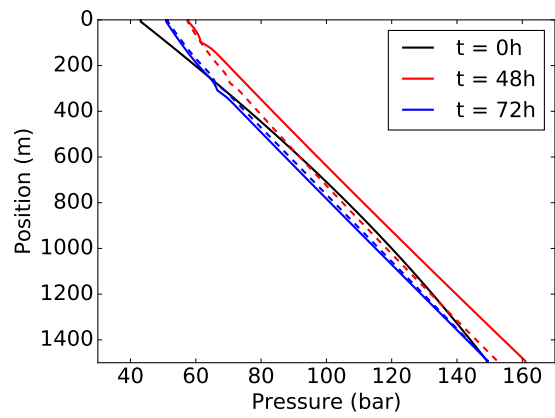
(d) Pressure, injection at $19.85\,^{\circ}\mathrm{C}$

Figure 4: The fluid temperature and pressure profiles initially (black), at the end of the first injection phase (red) and at the end of the first down-time (blue) for injection at $4.85\,^{\circ}\mathrm{C}$ (left) and $19.85\,^{\circ}\mathrm{C}$ (right). Solid and dashed lines show values for an injection mass flow of $100\,\mathrm{kg/s}$ and $25\,\mathrm{kg/s}$, respectively.
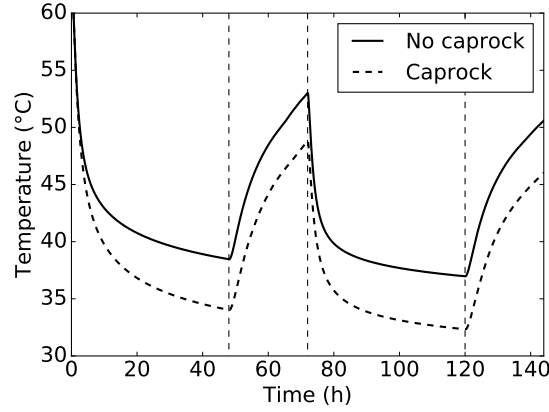
Figure 5: The time evolution of the casing temperature at 1450 m with and without a layer of caprock (properties given in Table 3) for a 48 h/24 h injection cycle with 4.85 °C CO_2 injected at a rate of 100 kg/s.
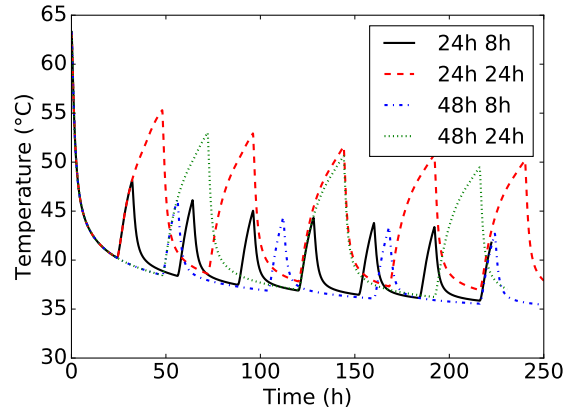
Figure 6: The time evolution of the casing temperature at 1450 m using different injection cycles when injecting 4.85 °C CO_2 at 100 kg/s.

a 24 h pause is not long enough for the casing temperature to recover to the temperature of the surrounding sandstone. Therefore, the pause interval is the main parameter affecting the max-min temperature difference of the injection cycle. However, both the injection and pause interval will affect the periodicity of the temperature evolution, which can be important for thermally induced stress in the materials involved.

6.2. Thermal stress

Cooling of the casing–cement–rock system below the initial formation temperature induces thermal stresses in casing, cement, and rock. In particular, the radial stress becomes less compressive as the casing and cement contract towards the axis of the well. If the radial stress at the casing–cement or cement–rock interface becomes tensile and sufficiently high, debonding will occur at the interface. Debonding may jeopardize well integrity if it creates a continuous flow path along the well. In this study, we evaluate thermal stresses induced by cyclic cooling of the casing's inner surface, as obtained from the flow and heat transfer model in Section 6.1.

A 2D thermoelastic finite-element model is set up in ABAQUS, representing a horizontal cross section of the well. The model has three sections: casing (inner diameter 0.222 m; outer diameter 0.244 m); cement

13

Table 5: Material properties used in the reference case for the thermal stress simulation.

Property	Unit	Casing (steel)	Cement	Rock
Density	kg/m^3	7850	1970	2600
Young's modulus	GPa	200	10	10
Poisson's ratio	(-)	0.2	0.15	0.2
Specific heat capacity	J/(kg K)	500	780	1000
Thermal conductivity	W/(m K)	40	0.72	2
Thermal expansion coefficient	10^{-6} K^{-1}	11	11	11

sheath (inner diameter 0.244 m, outer diameter 0.31 m) and rock (inner diameter 0.31 m). The outer dimensions of the model are 3 m × 3 m, i.e. sufficiently large to eliminate any boundary effects.

6.2.1. Material properties

Three cases were simulated:

- the reference case (Table 5);

- soft cement;

- increased contrast in the thermal expansion coefficient between casing and cement.

Material properties used in the reference case are listed in Table 5. In the reference case the Young's modulus of cement is equal to that of the rock. Moreover, the coefficient of thermal expansion has the same value for all materials in the reference case. In the soft cement case, the Young's modulus of cement was reduced by a factor of ten, i.e. from 10 GPa to 1 GPa. The Young's modulus of cement was thus ten times lower than the Young's modulus of the rock. This corresponds to flexible cement formulations quoted e.g. by Boukhelifa *et al.* (2005). Flexible cements are used in well cementing in order to prevent stresses from building up in cement. The purpose of simulating the soft cement case was to verify that such a cement formulation indeed may reduce the radial stresses and thereby lower the risk of debonding in the modelled CO_2 injection well.

In the simulation with enhanced contrast in the thermal expansion coefficient between casing and cement, the coefficient of thermal expansion of the casing material was set equal to 13×10^{-6} K^{-1}, as compared to 11×10^{-6} K^{-1} used in the reference case. All other parameters were kept unchanged and equal to those in the reference case.

Simulations were performed in drained conditions, i.e. it was assumed that there is no pore pressure change in cement and rock. In reality, contraction of the casing is likely to reduce the pore pressure in cement (because of two effects: higher thermal expansion coefficient of water than of rock, and poroelastic coupling between deformation and pore pressure, which would induce suction upon casing contraction). This will result in more compressive effective radial stresses than those predicted in our finite-element simulations. Our drained model thus provides a conservative estimate of well integrity under CO_2 injection.

6.2.2. Initial and boundary conditions

Two kinds of initial and boundary conditions must be specified for this model: thermal and mechanical. The initial temperature is assumed equal to 63.35 °C in the entire model. The external boundary of the model is held at 63.35 °C during the simulation (Dirichlet boundary condition). Since the external boundary is quite far from the well, assuming a Neumann boundary condition would not significantly affect the temperature and stress distribution in the near-well area. The temperature at the inner surface of the casing varies over time as shown in Figure 3. Only one injection scenario was simulated in the study of thermal stresses, namely the *worst-case* scenario giving the largest amplitude in downhole temperature variations (CO_2 temperature 4.85 °C, injection rate 100 kg/s, 24 h on, 24 h off).

Mechanical initial conditions are more difficult to specify in this problem. In particular, the initial compressive stresses in cement are not known. There is no agreement in the cement research community as

to how these stresses should be assigned in numerical models. For a detailed discussion on this topic, we refer to an extensive literature (Bosma *et al.*, 1999; Bois *et al.*, 2011; Lavrov and Torsæter, 2016; Fjær *et al.*, 1992). The initial state used in the present model is stress-free, and all stresses obtained in the analysis are to be considered as increments with regard to the (would-be) initial state of stress.

Mechanical boundary conditions in this study are the same as those routinely used in geomechanical modelling: the bottom side and the left-hand side boundaries of the 2D domain have zero normal displacements ("rollers"); normal stresses are applied at the top side and the right-hand side of the model. In this study, these stresses are set equal to zero since we only are interested in stress variations caused by the heating/cooling cycles. The inner surface of the casing is stress-free as well. These boundary conditions automatically produce a stress-free initial state of the model at the beginning of the simulation, just as we need. The model is plane strain, i.e. no deformations are allowed in the direction normal to the model plane (i.e. parallel to the pipe axis). This is a most common assumption in rock-mechanical well models (see e.g. Gray *et al.* (2009)), and it is valid as long as the well is sufficiently long and straight.

6.2.3. Results

Stress vs. time in the reference case is shown in Figure 7a. Tensile stresses are positive in Figure 7a. Thus, an increase in stress means that the stress in cement becomes less compressive (if it was compressive before injection) or more tensile (if it was close to zero). At the maximum drop in temperature (25 h after the beginning of the simulation), the radial stress at the casing–cement interface has increased by 1.8 MPa with regard to the initial stress. If the initial stresses are close to zero, this radial stress is most likely to induce debonding at the interface since tensile strength of cement–steel interfaces is below 1–2 MPa (Dusseault *et al.*, 2000). Tensile strength may even be as low as zero, e.g. if oil-based mud was in the hole when the casing was run in, and the mud film was not properly removed from casing's outer surface before pumping cement.

The radial stress is only slightly lower at the cement–rock interface than at the at the casing–cement interface. However, the cement–rock bonding is expected to be stronger than the steel–cement bonding (Evans and Carter, 1961). Therefore, the main concern in the reference case is debonding along the casing–cement interface. In order to prevent debonding, an expanded cement formulation could be used. This should create sufficiently high compressive initial stresses that the radial stress does not turn tensile during subsequent CO_2 injection.

The axial stress change in cement is on the order of 2–3 MPa at the peak of the cooling (blue and green curves in Figure 7a). If the initial axial stress was below 1–2 MPa, such stress change could induce disking of the cement sheath. However, the initial axial stress in the cement sheath is expected to be on the order of the hydrostatic weight of the cement column (and of whatever is above the column). The original hydrostatic pressure of the slurry column (with the overlaying fluids) would, in practice, be about 20 MPa at the depth modelled in this study (1450 m). This is the axial stress in cement before the set. After the set, the vertical stress would be somewhat reduced because of shrinkage, yield strength buildup and wall friction development (Chenevert and Jin, 1989). Nonetheless, it is highly unlikely that the axial stress in the cement sheath would drop as low as 3 MPa at the depth of 1450 m. The risk of cement sheath disking at 1450 m during CO_2 injection is therefore judged to be minimal. If, however, our analysis were conducted at smaller depths, the conclusions might be different (both because the hydrostatic pressure in cement is lower and the CO_2 flowing down the well is colder at shallow depths).

Stresses vs. time in the case of soft cement are shown in Figure 7b. Two major differences are evident in Figure 7b as compared to the reference case (Figure 7a):

- the change of the axial stress in cement is about five times smaller with soft cement;

- the change of the radial stress at the casing–cement interface is about two times smaller with soft cement.

Thus, soft cement reduces the risk of tensile failure and debonding in cement. This was the primary reason for introducing soft-cement formulations in well construction. It should be remembered, however, that the tensile strength of soft cements is usually lower than that of conventional cements. Thus, if the initial
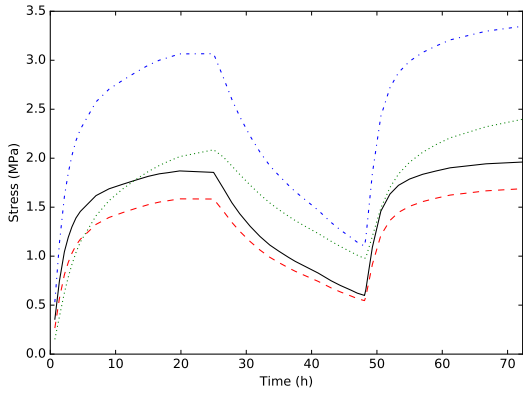
(a) Reference case
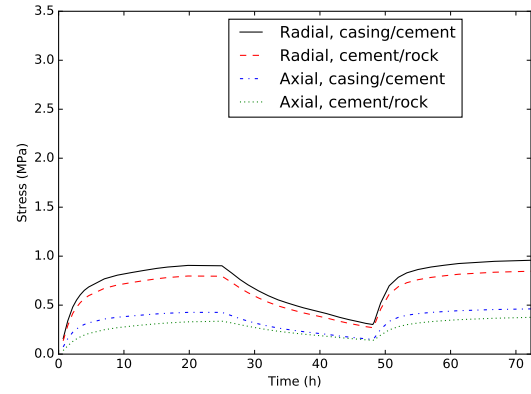
(b) Soft cement
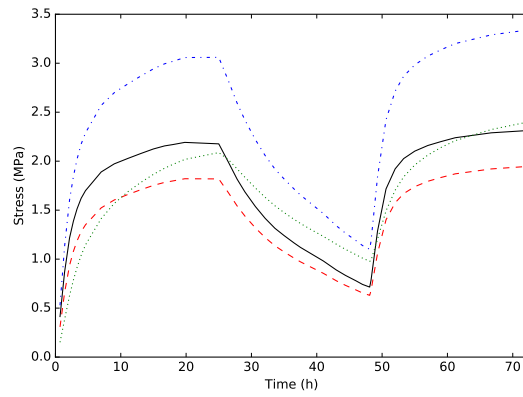
(c) Contrast in thermal expansion coefficient

Figure 7: Stress as a function of time during the two first cycles of an injection of $4.85\,^{\circ}$C CO_2 at $100\,\text{kg/s}$ for $24\,\text{h}$ followed by $24\,\text{h}$ down-time. Radial stress at the casing–cement interface (solid black), radial stress at the cement–rock interface (red dashed), axial stress at the casing–cement interface (blue dashed-dotted) and axial stress at cement–rock interface (dotted) are presented for the reference case, soft cement, and for increased contrast in the thermal expansion coefficient.

stresses are close to zero, the tensile radial stresses developing in soft cement (on the order of 0.3–0.4 MPa in Figure 7b) might be sufficient to create fractures in the bulk cement (or induce debonding). Thus, using soft cement still requires that sufficiently high initial compressive stresses exist in the cement sheath before the CO_2 injection starts.

Stress vs. time in the case of a contrast in the thermal expansion coefficient between casing and cement (casing having larger expansion coefficient than that of cement) are shown in Figure 7c. The changes of radial stresses induced at the casing–cement and cement–rock interfaces are slightly greater in this case than in the reference case (cf. Figure 7a). Qualitatively, this is rather obvious: a greater thermal expansion coefficient of the casing leads to greater casing contraction upon cooling. As a result, it applies a stronger pull on the cement sheath towards the borehole axis. This produces a greater reduction in the compressive radial stress in the cement sheath.

7. Conclusion

This paper has investigated CO_2 injection from ships and its impact on well integrity. The background for performing this study is the critical role that ship transport can play in delivering large volumes of CO_2 directly to offshore fields for the purposes of aquifer storage and/or enhanced oil recovery. There are still unanswered questions related to how the offloading of ships and injection should be performed at the site, and this study shows that well integrity considerations should be taken into account when choosing a solution.

We have carried out simulations of CO_2 injection cycles based on a ship-based North Sea storage scenario, by using a model that couples vertical two-phase flow of CO_2 and radial heat transfer between the injected CO_2 and the well in a realistic geometry. Specifically, we have studied the effect of injection temperature, injection flow rate, injection duration and down-time duration on the evolution of the casing temperature.

Our results reveal that the largest downhole temperature variations occur in the bottom section of the well, which is where the temperature difference between the injected fluid and the formation is at its largest. Within a realistic parameter space, it was found that the CO_2 injection scheme can be tailored to minimize loss of well integrity by careful selection of the following parameters:

- **Duration of injection:** The cooling of the well barriers during injection is so rapid that this parameter has little influence on well integrity.

- **Pause between intermittent injections (down-time):** The heat of the subsurface slowly heats the well, so this is a critical parameter. A long pause between injections gives the well time to heat to higher temperatures before it is cooled by another injection, which gives large temperature variations.

- **Temperature of injected CO_2:** This is a critical parameter since it directly affects the amplitude of temperature variations.

- **Rate of injection (mass flow):** This parameter also affects the degree of cooling – the higher the injection rate, the stronger the cooling.

In particular, for a low temperature injection at a high rate (4.85 °C and 100 kg/s) the bottom-hole temperature rise in the casing over the course of a 24 h down-time is estimated to more than 15 °C. A low-risk injection scheme with respect to downhole temperature variations is thus one where heated CO_2 is injected at low rates with minimal pauses between intermittent injectsion. This conflicts with direct offloading from single ships, and points towards intermediate storage on e.g. a floating storage and injection (FSI) vessel as a more viable solution.

The effect of a layer of shale caprock near the bottom hole was also investigated. If the bottom 100 m of the well is surrounded by caprock instead of by sandstone, then simulations indicate more cooling in the tubing and casing.

Using the casing temperature cycles obtained from the coupled fluid–heat simulations, we have estimated the radial and axial thermal stress at the casing–cement and cement–rock interface. Cooling of the casing in

the worst-case CO_2 injection scenario may reduce the compressive radial stress at the casing–cement interface by a few MPa. If the initial radial stress is not sufficiently compressive (because of e.g. cement shrinkage), such stresses may induce debonding at the casing–cement interface. In order to prevent debonding, it is recommended to use cement formulations that, after set, result in a softer cement. The probability of tensile failure (radial cracking) of the cement is also reduced by choosing a softer cement material. Moreover, the cement should be in a compressive state after set, and it should have a sufficiently high thermal expansion coefficient in order to prevent the pulling effect when the (much stiffer) casing contracts during cooling and pulls the cement sheath towards the borehole axis.

Since the initial stresses in the cement sheath increase with depth, while thermal stresses are only indirectly linked to the wellbore depth (by the CO_2 temperature being a function of depth), it might, paradoxically, be easier to prevent debonding at greater depths than at shallow depths. However, other factors, e.g. elevated formation temperatures, may have an adverse effect on well integrity in deep CO_2 wells.

In further work, other well material combinations could be investigated, to determine whether such combinations could reduce thermal stresses. Moreover, the benefits and potential issues of having intermediate CO_2 storage should be considered. Backflow of water when CO_2 is not injected may be another issue when CO_2 is injected intermittently, which could potentially cause corrosion. To determine whether this is a significant effect would require coupled well and reservoir simulations.

Appendix A. Nomenclature

Symbol	Description	Dimension	SI unit
A	Tubing cross-sectional area	L^2	m^2
c_p	Specific heat capacity at constant pressure	$L^2 T^{-2} \Theta^{-1}$	$\mathrm{m}^2/(\mathrm{s}^2\,\mathrm{K})$
E	Total energy density	$ML^{-1}T^{-2}$	$\mathrm{kg}/(\mathrm{m}\,\mathrm{s}^2)$
e_k	Phase specific internal energy	$L^2 T^{-2}$	$\mathrm{m}^2/\mathrm{s}^2$
f_{wall}	Wall friction density	$ML^{-2}T^{-2}$	$\mathrm{kg}/(\mathrm{m}^2\,\mathrm{s}^2)$
g	Gravity on well axis	LT^{-2}	m/s^2
h_i	Fluid–wall heat transfer coefficient	$MT^{-3}\Theta^{-1}$	$\mathrm{kg}/(\mathrm{s}^3\,\mathrm{K})$
I	Reservoir injectivity	LT	$\mathrm{m}\,\mathrm{s}$
p	Pressure	$ML^{-1}T^{-2}$	$\mathrm{kg}/(\mathrm{m}\,\mathrm{s}^2)$
Q	Heat transfer	$ML^{-1}T^{-3}$	$\mathrm{kg}/(\mathrm{m}\,\mathrm{s}^3)$
r	Radius from tubing centre	L	m
r_i	Tubing inner radius	L	m
t	Time	T	s
T	Temperature	Θ	$^\circ\mathrm{C}$
T_w	Wall temperature	Θ	$^\circ\mathrm{C}$
v	Fluid velocity	LT^{-1}	m/s
x	Distance along well	L	m
α_k	Phase volume fraction	$-$	$-$
κ	Thermal conductivity	$MLT^{-3}\Theta^{-1}$	$\mathrm{kg}\,\mathrm{m}/(\mathrm{s}^3\,\mathrm{K})$
ρ	Mixture mass density	ML^{-3}	kg/m^3
ρ_k	Phase mass density	ML^{-3}	kg/m^3

References

Albawi, A., 2013. *Influence of Thermal Cycling on Cement Sheath Integrity.* Master's thesis, Department of Petroleum Engineering and Applied Geophysics, Norwegian University of Science and Technology (NTNU).

Aspelund, A., Mølnvik, M. J., de Koeijer, G., 2006. Ship transport of CO_2: Technical solutions and analysis of costs, energy utilization, exergy efficiency and CO_2 emissions. *Chemical Engingeering Research & Design* 84 (9), 847–855. doi:10.1205/cherd.5147.

Aursand, E., Aursand, P., Hammer, M., Lund, H., 2016. The influence of CO_2 mixture composition and equations of state on simulations of transient pipeline decompression. *International Journal of Greenhouse Gas Control*, 54 (2), 599–609. doi:10.1016/j.ijggc.2016.07.004.

Bjørkevoll, K. S., 2014. Personal communication.

Bois, A.-P., Garnier, A., Galdiolo, G., Laudet, J.-B., 2010. Use of a mechanistic model to forecast cement-sheath integrity for CO_2 storage. In: *SPE International Conference on CO_2 Capture, Storage, and Utilization, 10-12 November, New Orleans, Louisiana, USA.* doi:10.2118/139668-MS.

Bois, A.-P., Garnier, A., Rodot, F., Sain-Marc, J., Aimard, N., 2011. How to prevent loss of zonal isolation through a comprehensive analysis of microannulus formation. *SPE Drilling & Completion* 26 (1), 13–31. doi:10.2118/124719-PA.

Bosma, M., Ravi, K., Van Driel, W., Schreppers, G. J., 1999. Design approach to sealant selection for the life of the well. In: *SPE Annual Technical Conference and Exhibition.* Society of Petroleum Engineers.

Boukhelifa, L., Moroni, N., James, S. G., Le Roy-Delage, S., Thiercelin, M. J., Lemaire, G., 2005. Evaluation of cement systems for oil and gas well zonal isolation in a full-scale annular geometry. In: *IADC/SPE Drilling Conference.* Dallas, Texas, USA. doi:10.2516/ogst/2012087. IADC/SPE 87195.

Brownsort, P., Jan. 2015. *Ship transport of CO_2 for Enhanced Oil Recovery – Literature Survey.* Tech. rep., Scottish Carbon Capture & Storage, Edinburgh, Scotland.

Cannon, J. R., 1984. *The One-Dimensional Heat Equation.* Encyclopedia of Mathematics and its Applications. Cambridge University Press. ISBN 9780521302432.

Carey, J. W., Wigand, M., Chipera, S., WoldeGabriel, G., Pawar, R., Lichtner, P., Wehner, S., Raines, M., Guthrie, G. D., Jr., 2007. Analysis and performance of oil well cement with 30 years of CO_2 exposure from the SACROC Unit, West Texas, USA. *International Journal of Greenhouse Gas Control* 1, 75–85. doi:10.1016/S1750-5836(06)00004-1.

Chenevert, M. E., Jin, L., 1989. Model for predicting wellbore pressures in cement columns. In: *SPE Annual Technical Conference and Exhibition.* Society of Petroleum Engineers.

Cronshaw, M. B., Bolling, J. D., Mar. 1982. A numerical model of the non-isothermal flow of carbon dioxide in wellbores. In: *SPE California Regional Meeting.* Society of Petroleum Engineers, San Francisco, California, USA. doi:10.2118/10735-MS. Paper SPE-10735-MS.

Crow, W., Carey, J. W., Gasda, S., Williams, D. B., Celia, M., 2010. Wellbore integrity analysis of a natural CO_2 producer. *International Journal of Greenhouse Gas Control* 4, 186–197. doi:10.1016/j.ijggc.2009.10.010.

De Andrade, J., Torsæter, M., Todorovic, J., Opedal, N., Stroisz, A., Vrålstad, T., Mar. 2014. Influence of casing centralization on cement sheath integrity during thermal cycling. In: *IADC/SPE Drilling Conference and Exhibition.* Society of Petroleum Engineers, Forth Worth, Texas, USA. doi:10.2118/168012-MS.

de Koeijer, G., Hammer, M., Drescher, M., Held, R., 2014. Need for experiments on shut-ins and depressurizations in CO_2 injection wells. In: Dixon, T., Herzog, H., Twinning, S. (Eds.), *GHGT-12 – 12th International Conference on Greenhouse Gas Control Technologies.* University of Texas at Austin / IEAGHGT, Energy Procedia, vol. 63, Austin, Texas, USA, pp. 3022–3029. doi:10.1016/j.egypro.2014.11.325.

Drew, D. A., Passman, S. L., 1999. *Theory of Multicomponent Fluids*, vol. 135 of *Applied Mathematical Sciences.* Springer-Verlag, New York. ISBN 0-387-98380-5.

Dusseault, M. B., Gray, M. N., Nawrocki, P. A., 2000. Why oilwells leak: cement behavior and long-term consequences. In: *International Oil and Gas Conference and Exhibition in China.* Society of Petroleum Engineers.

Eppelbaum, L., Kutasov, I., Pilchin, A., 2014. Thermal properties of rocks and density of fluids. In: *Applied Geothermics*, Springer Berlin Heidelberg, Lecture Notes in Earth System Sciences, pp. 99–149. ISBN 978-3-642-34022-2. doi:10.1007/978-3-642-34023-9_2.

Evans, G. W., Carter, L. G., 1961. Bonding studies of cementing compositions to pipe and formation. In: *API Drilling and Production Practice.* pp. 72–79.

Fenghour, A., Wakeman, W., V., V., 1998. The viscosity of carbon dioxide. *Journal of Physical and Chemical Reference Data* 27(1), 31–44. doi:10.1063/1.556013.

Fjær, E., Horsrud, P., Raaen, A. M., Risnes, R., Holt, R. M., 1992. *Petroleum related rock mechanics*, vol. 33. Elsevier.

Friedel, L., Jun. 1979. Improved friction pressure drop correlations for horizontal and vertical two phase pipe flow. In: *Proceedings, European Two Phase Flow Group Meeting.* Ispra, Italy. Paper E2.

Giljarhus, K. E. T., Munkejord, S. T., Skaugen, G., 2012. Solution of the Span-Wagner equation of state using a density-energy state function for fluid-dynamic simulation of carbon dioxide. *Industrial & Engineering Chemistry Research* 51 (2), 1006–1014. doi:10.1021/ie201748a.

Gilliam, T. M., Morgan, I. L., 1987. *Shale: Measurement of thermal properties.* Tech. rep., Oak Ridge National Laboratory.

Giorgis, T., Carpita, M., Battistelli, A., 2007. 2d modeling of salt precipitation during the injection of dry CO_2 in a depleted gas reservoir. *Energy Conversion and Management* 48 (6), 1816–1826. ISSN 0196-8904. doi:10.1016/j.enconman.2007.01.012. Geologic Carbon Sequestration and Methane Hydrates Research from the TOUGH Symposium 2006.

Gottlieb, S., Shu, C.-W., Tadmor, E., Mar. 2001. Strong stability-preserving high-order time discretization methods. *SIAM Review* 43 (1), 89–112. doi:10.1137/S003614450036757X.

Gray, K. E., Podnos, E., Becker, E., 2009. Finite-element studies of near-wellbore region during cementing operations: Part i. *SPE Drilling & Completion* 24 (01), 127–136. doi:10.2118/106998-PA.

Halliburton, 2012. N-SOLATE® High Performance Insulating Packer Fluids. URL http://www.halliburton.com/public/bar/contents/Data_Sheets/web/Sales_Data_Sheets/N-SOLATE.pdf [Online; accessed 29 September 2014].

Hammer, M., Ervik, Å., Munkejord, S. T., 2013. Method using a density-energy state function with a reference equation of state for fluid-dynamics simulation of vapor-liquid-solid carbon dioxide. *Industrial & Engineering Chemistry Research* 52 (29), 9965–9978. doi:10.1021/ie303516m.

Hammer, M., Morin, A., Sep. 2014. A method for simulating two-phase pipe flow with real equations of state. *Computers & Fluids* 100, 45–58. doi:10.1016/j.compfluid.2014.04.030.

Holt, R., Gheibi, S., Lavrov, A., 2016. Where does the stress path lead? Irreversibility and hysteresis in reservoir geomechanics. ARMA paper 16-496 presented at the 50th US Rock Mechanics / Geomechanics Symposium held in Houston, Texas, USA, 26-29 June 2016.

Kim, K.-Y., Han, W. S., Oh, J., Kim, T., Kim, J.-C., 2012. Characteristics of salt-precipitation and the associated pressure build-up during CO_2 storage in saline aquifers. *Transport in Porous Media* 92 (2), 386–418. doi:10.1007/s11242-011-9909-4.

Kjärstad, J., Skagestad, R., Eldrup, N. H., Johnsson, F., 2015. *Recommendations on CO_2 transport solutions.* Tech. rep. NORDICCS report D20, available at https://www.sintef.no/globalassets/sintef-energi/nordiccs/d20-recommendations-transport-abstract.pdf.

Kjøller, C., Torsæter, M., Lavrov, A., Frykman, P., 2016. Novel experimental/numerical approach to evaluate the permeability of cement-caprock systems. *International Journal of Greenhouse Gas Control* 45, 86–93. ISSN 1750–5836. doi:10.1016/j.ijggc.2015.12.017.

Krogh, E., Nilsen, R., Henningsen, R., 2012. Liquefied CO_2 injection modelling. *Energy Procedia* 23 (0), 527–555. ISSN 1876-6102. doi:10.1016/j.egypro.2012.06.022. The 6th Trondheim Conference on CO_2 Capture, Transport and Storage.

Lavrov, A., Torsæter, M., 2016. *Physics and Mechanics of Primary Well Cementing.* Springer.

LeVeque, R. J., 2002. *Finite Volume Methods for Hyperbolic Problems.* Cambridge University Press, Cambridge, UK. ISBN 0-521-00924-3.

Lindeberg, E., 2011. Modelling pressure and temperature profile in a CO_2 injection well. In: Gale, J., Hendriks, C., Turkenberg, W. (Eds.), *GHGT-10 – 10th International Conference on Greenhouse Gas Control Technologies.* IEAGHGT, Energy Procedia vol. 4, Amsterdam, The Netherlands, pp. 3935–3941. doi:10.1016/j.egypro.2011.02.332.

Lindeberg, E., Vuillaume, J.-F., Ghaderi, A., 2009. Determination of the CO_2 storage capacity of the utsira formation. In: Gale, J., Herzog, H., Braitsch, J. (Eds.), *GHGT-9 – 9th International Conference on Greenhouse Gas Control Technologies.*

Energy Procedia vol. 1, Washington DC, USA, pp. 2777–2784. doi:10.1016/j.egypro.2009.02.049.

Linga, G., Lund, H., 2016. A two-fluid model for vertical flow applied to CO_2 injection wells. *International Journal of Greenhouse Gas Control* 51, 71–80. doi:10.1016/j.ijggc.2016.05.009.

Lu, M., Connell, L. D., 2008. Non-isothermal flow of carbon dioxide in injection wells during geological storage. *International Journal of Multiphase Flow* 2 (2), 248–258. doi:10.1016/S1750-5836(07)00114-4.

Lu, M., Connell, L. D., 2014a. The transient behaviour of CO_2 flow with phase transition in injection wells during geological storage – Application to a case study. *Journal of Petroleum Science and Engineering* 124, 7–18. doi:10.1016/j.petrol.2014.09.024.

Lu, M., Connell, L. D., 2014b. Transient, thermal wellbore flow of multispecies carbon dioxide mixtures with phase transition during geological storage. *International Journal of Multiphase Flow* 63, 82–92. doi:10.1016/j.ijmultiphaseflow.2014.04.002.

Lund, H., Torsæter, M., Munkejord, S. T., 2016. Study of thermal variations in wells during CO_2 injection. *SPE Drilling & Completion* doi:10.2118/173864-PA.

Luo, Z., Bryant, S., 2013. Can we overcome thermo-elastic limits on CO_2 injection rates in horizontal wells? *Energy Procedia* 37, 3299–3306. ISSN 1876-6102. doi:10.1016/j.egypro.2013.06.218. GHGT-11 – 11th International Conference on Greenhouse Gas Control Technologies, 18-22 November 2012, Kyoto, Japan.

Maharaj, G., 1996. Thermal well casing failure analysis. SPE paper 36143 presented at the Fourth Latin American and Caribbean Petroleum Engineering Conference held in Port-of-Spain, Trinidad & Tobago, 23-26 April 1996.

Manceau, J. C., Tremosa, J., Audigane, P., Lerouge, C., Claret, F., Lettry, Y., Fierz, T., Nussbaum, C., 2015. Well integrity assessment under temperature and pressure stresses by a 1:1 scale wellbore experiment. *Water Resources Research* 51 (8), 6093–6109. ISSN 1944–7973. doi:10.1002/2014WR016786.

Mazzetti, M. J., Eldrup, N. H., Røkke, N. A., 2015. *NORDICCS CCS roadmap*. Tech. rep. Available at `https://www.sintef.no/globalassets/project/nordiccs/nordiccs-roadmap-updated-2015-12-033.pdf`.

Moumets, H., Polivach, Y., Zarmora, C. S., June 2015. *National Inventory Report (NIR) Snøhvit field 2014*. Tech. Rep. AU-SNO-00023, Statoil. Available at `http://www.miljodirektoratet.no/Global/dokumenter/horinger/Vedlegg%202%20-%20National%20Inventory%20Report%20(NIR)%20Sn%C3%B8hvit%20field%202014.pdf?epslanguage=no`.

Munkejord, S. T., Hammer, M., Jun. 2015. Depressurization of CO_2-rich mixtures in pipes: Two-phase flow modelling and comparison with experiments. *International Journal of Greenhouse Gas Control* 37, 398–411. doi:10.1016/j.ijggc.2015.03.029.

Munkejord, S. T., Hammer, M., Løvseth, S. W., May 2016. CO_2 transport: Data and models – A review. *Applied Energy* 169, 499–523. doi:10.1016/j.apenergy.2016.01.100.

Munkejord, S. T., Jakobsen, J. P., Austegard, A., Mølnvik, M. J., Jul. 2010. Thermo- and fluid-dynamical modelling of two-phase multi-component carbon dioxide mixtures. *International Journal of Greenhouse Gas Control* 4 (4), 589–596. doi:10.1016/j.ijggc.2010.02.003.

Musivand Arzanfudi, M., Al-Khoury, R., 2015. A compressible two-fluid multiphase model for CO_2 leakage through a wellbore. *International Journal for Numerical Methods in Fluids* 77 (8), 477–507. doi:10.1002/fld.3990.

Norwegian Ministry of Petroleum and Energy, 2015. CCS: Pre-feasibility study on potential full-scale projects in Norway delivered. News story. URL `https://www.regjeringen.no/en/aktuelt/id2410129/`.

Norwegian Ministry of Petroleum and Energy, 2016. Initiates feasibility study on subsea CO_2 storage. Press release (No: 001/16). URL `https://www.regjeringen.no/en/aktuelt/id2469150/`.

Nygaard, R., Salehi, S., Weideman, B., Lavoie, R. G., 2014. Effect of dynamic loading on wellbore leakage for the wabamun area CO_2 sequestration project. *Journal of Canadian Petroleum Technology* 53, 69–82. doi:10.2118/146640-PA.

Pan, L., Oldenburg, C. M., Wu, Y.-S., Pruess, K., 2009. Wellbore flow model for carbon dioxide and brine. In: Gale, J., Herzog, H., Braitsch, J. (Eds.), *GHGT-9 – 9th International Conference on Greenhouse Gas Control Technologies*. MIT / IEA GHG, Energy Procedia vol. 1, Washington DC, USA, pp. 71–78. doi:10.1016/j.egypro.2009.01.012.

Paterson, L., Lu, M., Connell, L., Ennis-King, J. P., Sep. 2008. Numerical modeling of pressure and temperature profiles including phase transitions in carbon dioxide wells. In: *SPE Annual Technical Conference and Exhibition*. Society of Petroleum Engineers, Denver, Colorado, USA. doi:10.2118/115946-MS. Paper SPE-115946-MS.

Peng, D. Y., Robinson, D. B., Feb. 1976. A new two-constant equation of state. *Industrial & Engineering Chemistry Fundamentals* 15 (1), 59–64. doi:10.1021/i160057a011.

Ruan, B., Xu, R., Wei, L., Ouyang, X., Luo, F., Jiang, P., 2013. Flow and thermal modeling of CO_2 in injection well during geological sequestration. *International Journal of Greenhouse Gas Control* 19, 271–280. doi:10.1016/j.ijggc.2013.09.006.

Span, R., Wagner, W., Nov.–Dec. 1996. A new equation of state for carbon dioxide covering the fluid region from the triple-point temperature to 1100 K at pressures up to 800 MPa. *Journal of Physical and Chemical Reference Data* 25 (6), 1509–1596. doi:10.1063/1.555991.

Søreide, O., Hansen, S., Stenebråten, J., 2014. Estimation of reservoir stress effects due to injection of cold fluids: an example from ncs. ARMA paper 12-7394 presented at the 48th U.S. Rock Mechanics/Geomechanics Symposium held in Minneapolis, Minnesota, 1-4 June 2014.

Thu, E. S., 2013. *Modeling of Transient CO_2 Flow in Pipelines and Wells*. Master's thesis, Department of Energy and Process Engineering, Norwegian University of Science and Technology (NTNU).

Toro, E. F., Billett, S. J., Nov. 2000. Centred TVD schemes for hyperbolic conservation laws. *IMA Journal of Numerical Analysis* 20 (1), 47–79. doi:10.1093/imanum/20.1.47.

Vermeulen, T. N., Jun. 2011. *Knowledge Sharing Report - CO_2 Liquid Logistics Shipping Concept (LLSC): Overall Supply Chain Optimization*. Tech. rep., Global CCS Institute, Anthony Veder, Vopak.

Vesovic, V., Wakeham, W., Olchowy, G., Sengers, J., Watson, J., Millat, J., 1990. The transport properties of carbon dioxide. *Journal of Physical and Chemical Reference Data* 19, 763–808. doi:10.1063/1.555875.

Whiriskey, K., 2014. *Scaling the CO_2 storage industry: A study and a tool*. Tech. rep., Bellona. URL `http://bellona.org/assets/sites/4/Scaling-the-CO2-storage-industry_Bellona-Europa.pdf`